Five-Dimensional Potential-Energy Surfaces and Coexisting Fission Modes in Heavy Nuclei

Peter Möller*, David G. Madland*, Arnold J. Sierk*, and A. Iwamoto†

*Theoretical Division, Los Alamos National Laboratory, Los Alamos, New Mexico 87545, USA
†Department of Materials Sciences, Japan Atomic Energy Research Institute, Tokai-mura, Naka-gun, Ibaraki, 319-1195 Japan

Abstract. We calculate complete fission potential-energy surfaces versus five shape coordinates: elongation, neck diameter, light-fragment deformation, heavy-fragment deformation, and mass asymmetry for even nuclei in the range $82 \leq Z \leq 100$. The potential energy is calculated in terms of the macroscopic-microscopic model with a folded-Yukawa single-particle potential and a Yukawa-plus-exponential macroscopic model in the three-quadratic-surface parameterization. The structure of the calculated energy landscapes exhibits multiple valleys leading to different scission configurations. The properties of these valleys and the saddle-points at the beginning of these valleys can be directly related to bimodal fission properties observed in the radium region, in the light-actinide region, and in the fermium region[1−4]). The rms deviation between calculated and experimental fission-barrier heights is only 1.08 MeV for 31 nuclei from ^{70}Se to ^{252}Cf.

INTRODUCTION

When a heavy nucleus divides into two fragments in nuclear fission, two key aspects of the process have challenged researchers since the discovery of fission more that 60 years ago. First, what is the threshold energy for the reaction and, second, what are the shapes involved in the transition from a single nuclear system to two separated daughter fragment nuclei? These two questions are intimately connected. The energy of a nucleus as a function of shape defines a landscape in a multi-dimensional deformation space. It is the energy of the lowest mountain pass, or saddle-point, in this landscape, connecting the nuclear ground state with the region corresponding to separated fragments that represents the threshold energy of the fission process.

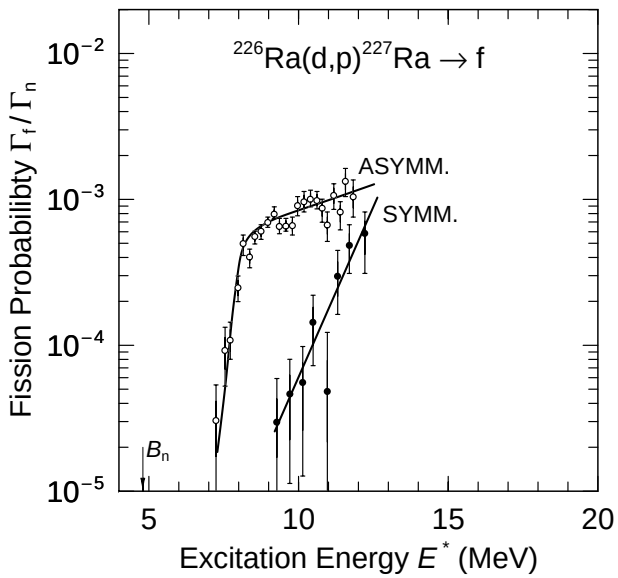

FIGURE 1. Fission probability data show different thresholds for mass-asymmetric and mass-symmetric fission near ^{227}Ra. The figure is based on a figure in Ref. [1]).

However, despite many fission potential-energy-surface calculations over the years certain features of the fission process have remained unexplained. For example:

1. Nuclei near ^{228}Ra exhibit two fission modes. We show in Fig. 1 an example of the extensive data obtained in Ref. [1]). In one mode, with the lower threshold energy, the fragment mass distribution is asymmetric and the fragment total kinetic energy is about 10 MeV higher than in the other, symmetric mode. The kinetic energies indicate that the scission configuration is more compact for the asymmetric mode than for the symmetric mode. From the totality of the data Ref. [1]) concludes: "Thus it seems that after the gross determination of the symmetric or asymmetric character of fission made already at the barrier, the two components follow a different path with no or little overlap in the development from the barrier to the scission configuration."

2. Most actinide nuclei near the line of β-stability undergo mass-asymmetric fission. From Th to Fm the heavy fragment mass is close to 140, with the remainder of the mass in the light fission fragment.

3. Near the far end of the actinide region fission properties change suddenly and sometimes exhibit a two-mode character in the same nucleus. For example, the fragment mass distribution changes abruptly from mass-asymmetric for ^{256}Fm to mass-symmetric for ^{258}Fm along with a correlated increase in the fragment total kinetic energy (TKE) by about 35 MeV. But ^{258}Fm also exhibits the asymmetric mode with lower TKE with a small probability: fission of such nuclei is characterized as bimodal.

Over the past decades many calculations based on 1000 or so grid points have been presented. However, to properly describe the evolution of a single nuclear

shape into two fragments of different mass and deformation, for example one spherical ^{132}Sn-like fragment and one deformed fragment, we have concluded that complete deformation spaces based on at least five independent shape parameters are required [5]). This leads to multi-million grid-point spaces.

SHAPE PARAMETERIZATION

Because fragment shell effects strongly influence the structure of the fission potential-energy surface long before scission, often in the outer saddle region, it is crucial to include in calculations the nascent-fragment deformations as two independent shape degrees of freedom. In addition, elongation, neck diameter, and mass-asymmetry shape-degrees of freedom are required, at a minimum, to adequately describe the complete fission potential-energy surface. For nascent-fragment deformations we choose spheroidal deformations characterized by Nilsson's quadrupole ϵ parameter. This single fragment-deformation parameter is sufficient because higher-multipole shape-degrees of freedom are usually of lesser importance in the fission-fragment mass region below the rare earths.

The three-quadratic-surface parameterization (3QS) is ideally suited for the above description. [6]) In the 3QS the shape of the nuclear surface is specified in terms of three smoothly joined portions of quadratic surfaces of revolution. Using this parameterization we here construct, calculate, and investigate complete five-dimensional spaces with 2 610 885 grid points as illustrated in Fig. 2.

A common notation used to characterize the fragment mass asymmetry of a fission event is $M_{\rm H}/M_{\rm L}$ where $M_{\rm H}$ and $M_{\rm L}$ are the masses of the heavy and light fission fragments respectively. For the purpose of grid generation for the potential-energy calculation it is convenient to relate a mass-asymmetry shape degree of freedom for the pre-scission nucleus to the final fission-fragment mass asymmetry in some fashion, although the final mass division, strictly speaking, cannot be determined from the static shapes occurring before scission. However, the exact nature of our definition of mass asymmetry for a single shape has little effect on the calculated saddle-point energies and shapes because our five-dimensional grid covers all of the physically relevant space available to the 3QS parameterization, regardless of how we choose to define a "mass-asymmetry" coordinate. In order to obtain a definition of mass asymmetry that is meaningful close to scission, and equations that are reasonably simple to work with for the purpose of grid-point generation, we define an auxiliary grid mass-asymmetry parameter $\alpha_{\rm g}$

$$\alpha_{\rm g} = \frac{M_1 - M_2}{M_1 + M_2} \tag{1}$$

where M_1 and M_2 are the volumes inside the end-body quadratic surfaces, were they completed to form closed-surface spheroids. Thus

$$\alpha_{\rm g} = \frac{a_1^2 c_1 - a_2^2 c_2}{a_1^2 c_1 + a_2^2 c_2} \tag{2}$$

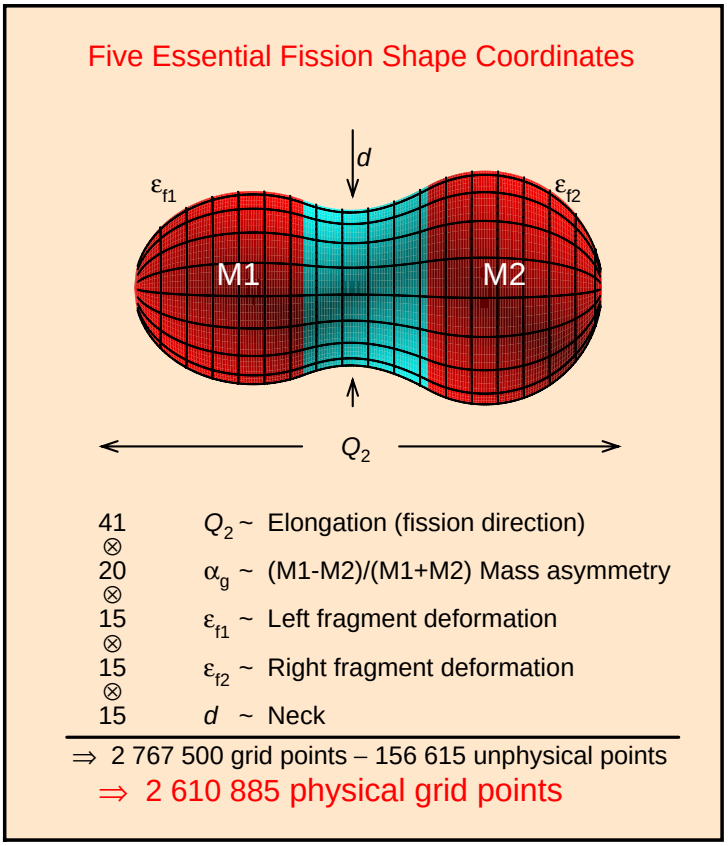

FIGURE 2. Five-dimensional shape parameterization used in our potential-energy calculation. Different colors indicate the three different quadratic surfaces of the shape parameterization used in our calculation. The first derivative is continuous at the intersections of the surfaces. For the nascent spheroidal fragments we characterize the deformations by Nilsson's quadrupole ϵ parameter. Shapes corresponding to certain quadrupole moments do not exist for specific combinations of the other shape parameters. For example, zero quadrupole moment cannot be realized for shapes with very deformed ends. In our grid there exist $156\,615$ such "unphysical" points. Thus, we are left with $2\,610\,885$ shapes for which we actually calculate the potential energy.

where a denotes the transverse semi-axis and c the semi-symmetry axis of the left (1) and right (2) quadratic surfaces of revolution. With this definition we select 20 coordinate values corresponding to

$$\alpha_g = -0.02 \ldots (0.02) \ldots 0.36 \tag{3}$$

We have closely spaced the asymmetry coordinate so that we will be able to spot favorable saddle-point shapes that may not appear in a more sparsely spaced grid. For ^{240}Pu the values 0.00, 0.02, and 0.36 of the mass-asymmetry coordinate α_g correspond to the mass divisions $120/120$, $122.4/117.6$, and $163.2/76.8$, respectively.

Because of the intuitive appeal of the notation $M_{\rm H}/M_{\rm L}$ we use it below to characterize the "asymmetry" of a single shape. We then connect $M_{\rm H}$ and $M_{\rm L}$ to $\alpha_{\rm g}$ through

$$M_{\rm H} = A\frac{1+\alpha_{\rm g}}{2} \quad \text{and} \quad M_{\rm L} = A\frac{1-\alpha_{\rm g}}{2} \tag{4}$$

for a nucleus with A nucleons. For shapes with a well-developed neck the ratio obtained with this definition can be expected to be close to the final fragment mass-asymmetry ratio. We cannot conveniently use M_1 and M_2 to designate the final fragment mass asymmetries because they do not exactly sum up to the total nuclear volume or mass. Equation (4) simply represents a scaling of M_1 and M_2 so that their sum after scaling adds up to the total mass number A.

ANALYSIS OF FIVE-DIMENSIONAL SPACES

It is a common misconception that the structure of a multi-dimensional potential-energy function can be determined by calculating and displaying the function versus two shape variables, for example, β_2 and β_3 where the function has been "minimized" with respect to additional multipoles such as β_4, β_5, β_6 and β_7.

Figure 3 illustrates, in two dimensions, some of the difficulties that occur in such a search for the relevant fission threshold saddle points in a multidimensional potential-energy landscape. Let Θ represent a coordinate in the fission direction and α all other coordinates and furthermore let the blue area at $\Theta = -100$ and $\alpha = 6.0$ represent the second minimum in the fission potential energy surface. And let the blue area to the right represent the valley of separated fission fragments. In many calculations based on "minimizations" with respect to additional coordinates the procedure would now be to increase the fission coordinate Θ by some increment, which for clarity we choose to be as large as 40, while keeping the additional shape-degrees of freedom fixed. This would take us along the initial part of the thin horizontal line to $\Theta = -60$ and $\alpha = 6.0$. Starting from this position the energy would now be minimized for fixed $\Theta = -60$. This would take us down to the large black dot on the dot-dashed line. The process would then be repeated with the result that the energy would be obtained for the succession of black dots on the dot-dashed line. Thus the energy that is obtained is the energy along the dot-dashed line. In our example here all the shape coordinates along this trajectory would vary continuously and no suspicion may arise that the saddle point found, in the region of the red arrow, *is not* the true saddle point, that is, it is not the *lowest* pass leading to the fission valley of separated fragments to the right in the figure. A minimum-energy trajectory should instead take us over the saddle-points identified by the green arrows in the figure. We can easily "see" this in a two-dimensional case as the example here, but in a higher-dimensional space it takes a clever algorithm to identify all of the relevant structure. This requirement led to the water-flow algorithm described below.

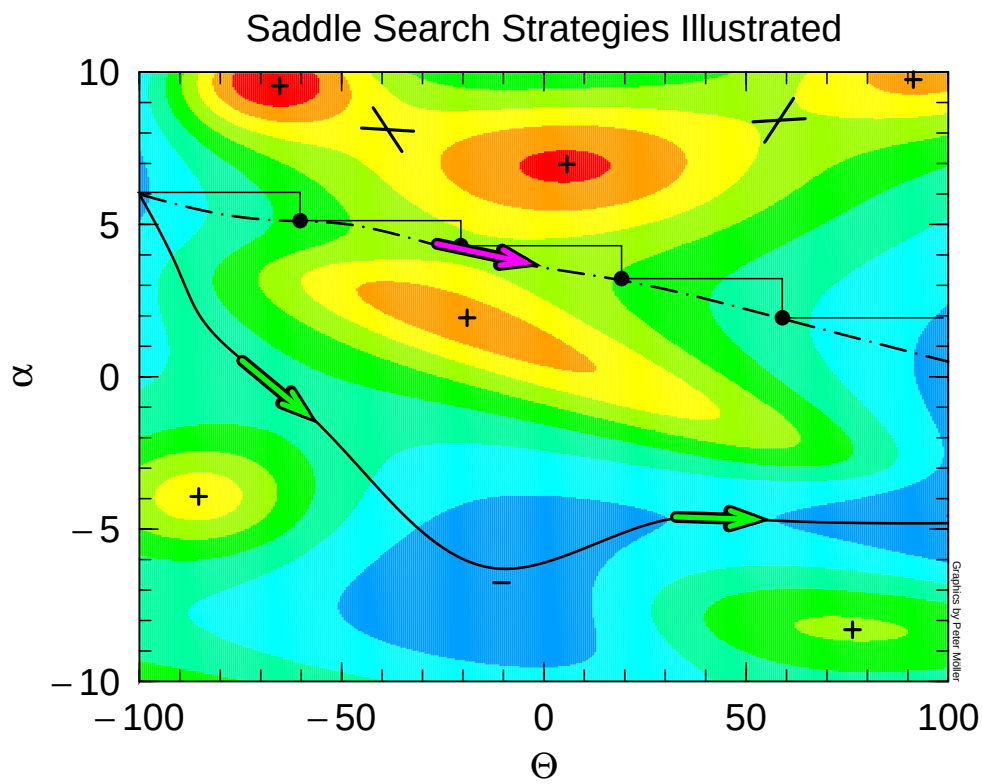

FIGURE 3. Maxima (+), minima (−), and saddle points (arrows or crossed lines) of a two-dimensional function. As discussed in the text it is not possible to obtain a lower-dimensional representation of this surface by "minimizing" with respect to the "additional" α shape-degree of freedom.

A numerical algorithm that locates the saddle points by the criteria that all first derivatives be zero and that the second derivatives have the appropriate signs would locate the saddles marked by crossed lines in the upper part of the figure in addition to the saddles we have already discussed. It would then be difficult to determine if any of these represented the lowest mountain pass between the second minimum and the blue area to the right representing the fission valley of separated fragments. However, as we will show the water-flow method simply bypasses these saddle points.

It is *also* a common misconception that *constrained* self-consistent calculations, for example HF or HFB calculations with Skyrme or Gogny forces [7−9]) automatically take into account all non-constrained variables. For the application to saddle-point determination this is incorrect. A self-consistent calculation constrained in one variable, for example Q_2, would have difficulties similar to those discussed above.

In addition, it is of interest to note that in calculations where the potential energy is displayed as contour diagrams versus two shape variables and in which the energy is minimized with respect to additional multipoles, only relatively few points are

required to perform a minimization with respect to, say, 3 additional multipoles, about 30 or so. If the two-dimensional contour diagram is based on 10 by 10 points then only 3 000 points are considered in the calculation. In contrast, we find that to adequately investigate the structure associated with five simultaneous shape-degrees of freedom almost 3 000 000 grid points, that is, 1000 *times* more points than earlier calculations purporting to be multi-dimensional are required.

The technique we use here to investigate the structure of the multidimensional surface is to employ imaginary water flows [5,10]) in the calculated 5-dimensional potential energy surface. For example, we imagine that we stepwise flood, in intervals of 1 MeV, the second minimum with water. During the flooding process we check at what water level a preselected "exit" grid point that is clearly in the fission valley near scission gets "wet". When this happens, then the water level has passed the threshold energy level for fission. We can determine the saddle-point energy to desired accuracy by repeating the filling procedure with successively smaller stepwise increases of the water level. In the second such iteration we only need to start the filling procedure at 1 MeV below the level for which the exit point became wet in the first iteration with its 1 MeV stepwise increases in the flooding level, and we then use a 0.1 MeV stepwise increase in the water level. Once the exit point again gets flooded we can again repeat the procedure with a smaller stepwise water-level increase until we have determined the saddle-point energy to desired accuracy. The saddle-point shape can also be obtained from this procedure.

Once the threshold energies for fission have been identified, it is of interest to establish if structure effects in the potential energy provide a mechanism for multi-mode fission, such as the well-known three-peaked mass distribution in ^{228}Ra fission [1]). To look for such structures we ask if there are valleys of distinctly different character running in the fission direction of increasing Q_2. For 10 or more fixed Q_2 values beyond the outer saddle region, we determine all minima in the remaining 4-dimensional space of the two fragment deformations, neck size and mass asymmetry. We find that there are usually two (but sometimes more) distinct valleys in the region beyond the second saddle region, one corresponding to a mass asymmetry $\alpha_{\rm g}$ of about $[140-(A-140)]/A$ and one corresponding to mass symmetry $\alpha_{\rm g} = 0$. To understand the significance of these valleys it is necessary to study their interconnections in the five-dimensional deformation-energy space.

Variations of the flooding algorithm allow us to determine that separate saddle points provide entries to the two valleys and the respective energies of these saddle points. Once the lowest saddle has been determined we may block the water flow across this saddle by building an imaginary dam across the saddle region. We can also totally block the water flow beyond a selected maximum Q_2. This prevents water from flowing down one valley and up "the back way" into the other valley. To determine the height of the ridge between the two valleys along their entire length we study for each fixed Q_2 the remaining 4-dimensional space in which the two valleys correspond to two minima and the ridge to the saddle separating them. We use the flooding algorithm in four dimensions to localize this saddle/ridge.

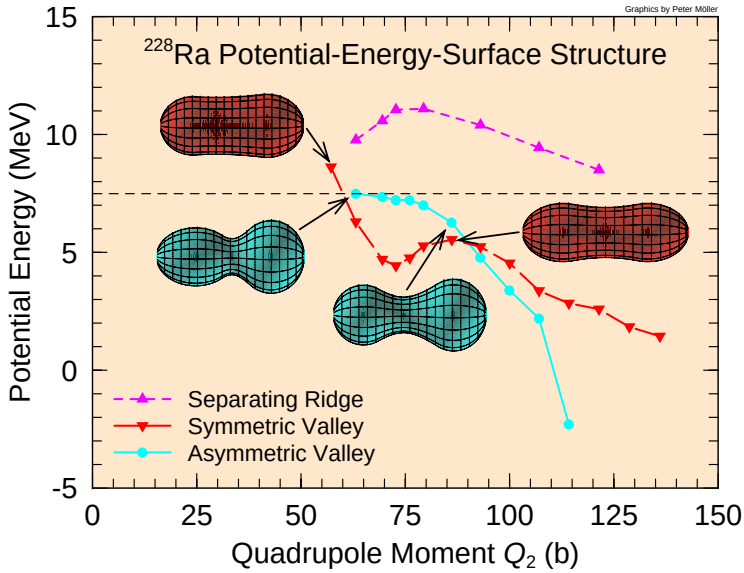

FIGURE 4. Potential-energy valleys and ridges and corresponding nuclear shapes for ^{228}Ra. The first point on each of the two curves with the label "valley" are actually saddle-points at the entrance to the valley that emerges beyond the saddle point. It is of interest to note that the entrance to the symmetric valley is slightly asymmetric. The subsequent points in this valley correspond to symmetric or very nearly symmetric shapes. The entry saddle-point to the symmetric valley is 1.13 MeV higher than the entry saddle-point to the asymmetric valley. The highest point on the separating ridge is 2.47 MeV higher than the symmetric saddle. The thin dashed line represents the threshold energy for fission. All energies are given relative to the spherical macroscopic energy.

RESULTS

We have calculated five-dimensional potential-energy surfaces for 138 even-even nuclei from Pb to Fm. We are currently subjecting these surfaces to various types of imaginary water-flow analyses as discussed in the previous section.

As examples of the structures we have found in the calculated 5-dimensional surfaces we show in Figs. 4 and 5 some fission-valley and separating-ridge features obtained for ^{228}Ra and ^{232}Th. The first point on the fission-valley potential-energy curves in Figs. 4 and 5 is the saddle point for entry into the particular valley. The nuclear shapes corresponding to the saddle points are shown to the left in the figure. Shapes corresponding to the symmetric and mass-asymmetric valleys at $Q_2 = 86$ b are shown to the right. Note that the shape corresponding to the *entry* to the mass-*symmetric* valley is slightly mass-*asymmetric*. The thin dashed line is the calculated threshold potential energy for fission which, to be consistent with the other curves, is given relative to the spherical macroscopic energy.

The calculated structure of the potential-energy surface therefore is consistent with the observed bimodal fission features in this region of nuclei [1,2]). The high ridge separating the two valleys for ^{228}Ra is peaked at 2.47 MeV above the en-

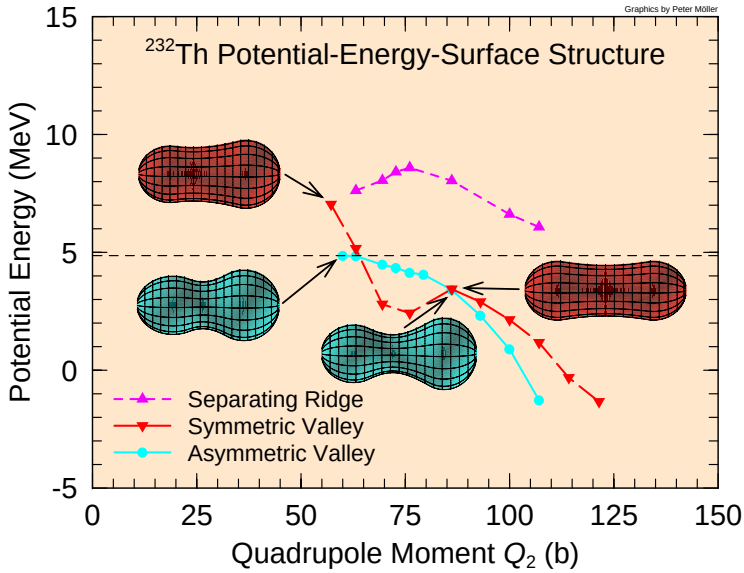

FIGURE 5. Potential-energy valleys and ridges and corresponding nuclear shapes for ^{232}Th. The first point on each of the two curves with the label "valley" are actually saddle-points at the entrance to the valley that emerges beyond the saddle point. It is of interest to note that the entrance to the symmetric valley is slightly asymmetric. The subsequent points in this valley correspond to symmetric or very nearly symmetric shapes. The entry saddle-point to the symmetric valley is 2.17 MeV higher than the entry saddle-point to the asymmetric valley. The highest point on the separating ridge is 1.56 MeV higher than the symmetric saddle. The thin dashed line represents the threshold energy for fission. All energies are given relative to the spherical macroscopic energy.

trance saddle to the symmetric valley. It therefore keeps the mass-symmetric and mass-asymmetric modes well separated up to scission, which is consistent with the experimentally observed data discussed in the introduction. Compare also with Fig. 1. Our results in Fig. 4 are *also* consistent with the observed total fragment kinetic energies which are about 10 MeV higher for asymmetric fission than for symmetric fission for several nuclei in this region [1]).

For ^{232}Th the lower separating ridge, peaked at 1.56 MeV above the entrance saddle to the symmetric valley, allows the symmetric component to partially revert back to the asymmetric valley before scission for ^{232}Th. Therefore, there is only a very weak symmetric fission component in low-energy fission of ^{232}Th. We find that the existence of at least two paths in the five-dimensional surface is a general result for nuclei in this region and we are now studying their relative importance over the large range of nuclei for which we have calculated potential-energy surfaces. We note that experimental fission data in the light-actinide region are currently interpreted in terms of two fission paths, one mass symmetric and the other mass asymmetric. The saddle leading to mass-symmetric division is observed to be 1 to 2 MeV higher than the saddle leading to mass-asymmetric division for nuclei in this region, in excellent agreement with our calculated potential-energy surfaces. Also, the experimental total fragment kinetic energies are higher in asymmetric

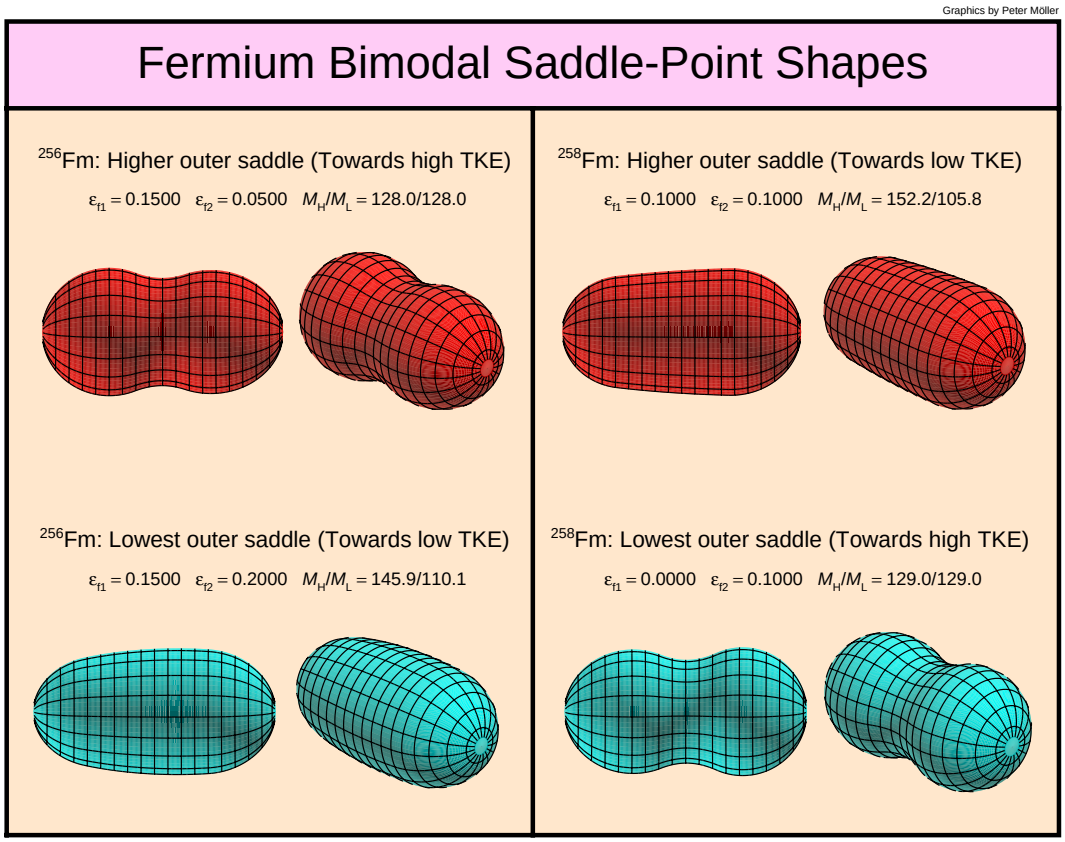

FIGURE 6. Bimodal saddle-point shapes for ^{256}Fm and ^{258}Fm.

fission than in symmetric fission. These observations [2,3]) are consistent with the compact and elongated shape configurations that we obtain in the corresponding fission valleys.

Turning to the heavy actinides, nuclei in the region near ^{258}Fm also exhibit bimodal features in fission as discussed in Ref. [4]). We have earlier tentatively identified bimodal structures in calculated *two-dimensional* potential-energy surfaces [11,12]), but only now can we verify that these interpretations are still valid when the calculation is taken from two to five dimensions. In the Fm region we have used one of the imaginary water-flow techniques described previously, namely the dam method, to find alternative saddle points that are higher in energy than the lowest threshold saddle point. For ^{256}Fm and ^{258}Fm we find the two distinct classes of saddle points shown in Fig. 6. For ^{256}Fm the shape of the lowest saddle indicates it corresponds to normal, low-TKE fission similar to what is observed in fission of slightly lighter actinides. However, another saddle point exists, which we calculate to be 0.30 MeV higher than the lower saddle point. This may correspond to fission into compact scission configurations with high kinetic energies. For ^{258}Fm the latter type of saddle-point becomes the lowest saddle point. Thus, we reproduce the experimentally observed transition point between asymmetric low-TKE fission and symmetric high-TKE fission as observed experimentally [4]).

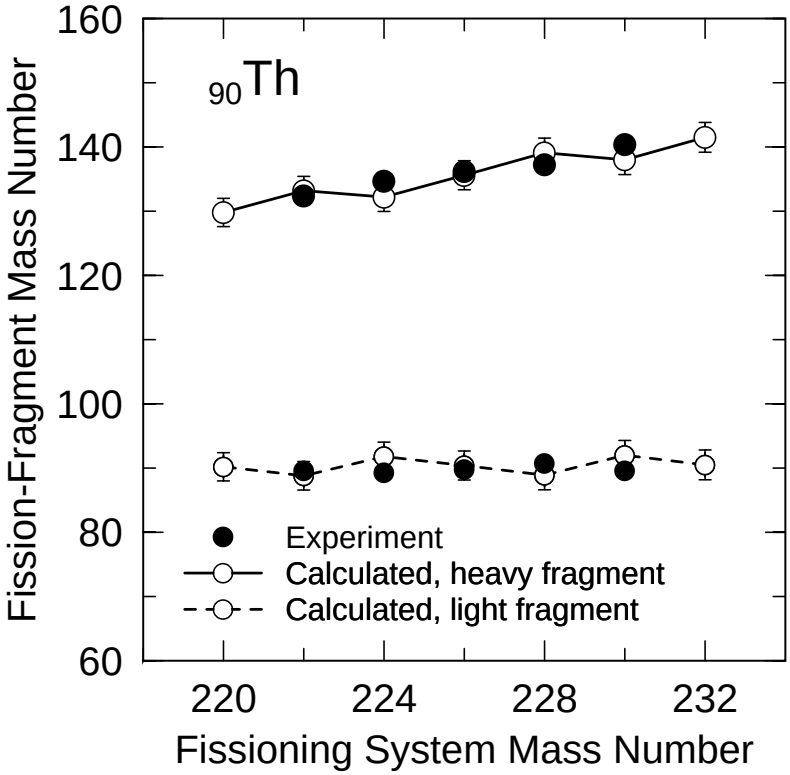

FIGURE 7. Calculated (open symbols) and measured (closed symbols) average mass division in asymmetric fission for a sequence of even isotopes of Th. The error bars on the calculated points correspond to the spacing of mass asymmetry values on the multidimensional shape-coordinate grid. The data is for spontaneous fission when it is available, otherwise data for low-energy induced fission is used. The results reproduce the experimental observation of a heavy fragment at mass number $A \sim 140$ and a light fragment with mass corresponding to the remainder of the original nucleus. However, deviations from this rule of thumb are also reproduced by the calculations.

As pointed out in the Introduction, it is a long-standing observation that in binary fission actinide nuclei preferentially divide into one fragment of about mass 140 and a complementary, smaller fragment of mass $A - 140$, where A is the mass number of the original nucleus. We show in Fig. 7 our calculated results for the fragment masses for the mass-asymmetric valley in fission for seven thorium isotopes. The data are from Refs. [13–15]). For all isotopes we have identified the fission valley corresponding to mass-asymmetric fission at $Q_2 = 99$ b. The value of the mass-asymmetry coordinate $\alpha_{\rm g}$ at the valley bottom directly yields the mass of the heavy and light fission fragments according to Eq. (4). The "valley floor" corresponds to a local minimum in the four-dimensional space remaining when Q_2 is fixed at a specific value. In Fig. 8 we have plotted the charge asymmetry for some isotopes of Th and U, cf. Ref. [15]). We observe that the charge of the heavy fragment remains constant, whereas there is a substantial variation in the heavy-fragment neutron number along the Th and U isotope chains.

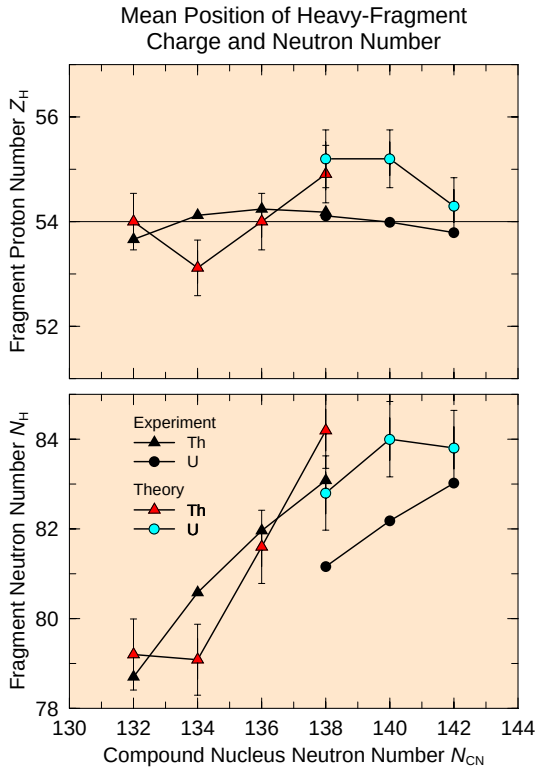

FIGURE 8. Calculated proton number and neutron number of the heavy fission fragment of isotopes of Th and U compared to experiment for the mass-asymmetric fission mode. The error bars correspond to the spacing of the mass-asymmetry shape coordinate.

Our results in this paper are based on calculations with the FRLDM 1992 parameter set [16]). Because of our expanded and more realistic deformation space our calculated barrier heights are systematically lowered relative to earlier, limited-space calculations. To obtain optimum agreement with experiment a readjustment of the FRLDM model parameters is therefore necessary. We have recently performed such a readjustment of the FRLDM model parameters to nuclear ground-state masses and barrier heights in the manner described in Ref. [16]). We obtain an overall barrier rms error of only 1.08 MeV and an overall mass model error of 0.759 MeV. The new calculated and experimental barrier heights are listed in Table 1.

SUMMARY

Our current analysis of the new calculated potential energy landscapes in five dimensions allows us to draw the following conclusions:

1. Multiple fission paths are found for most nuclei in the mass range considered.

2. For radium and light actinide nuclei two paths dominate: one mass-asymmetric and one mass-symmetric. These paths correspond to different fission modes, such as those illustrated in Fig. 1 in the Introduction.

TABLE 1

Calculated "outer" barrier heights compared to experimental barrier data, after readjustment of the macroscopic-model constants. For proton number below 80 the barriers are the macroscopic barriers. A typical experimental barrier uncertainty is 1 MeV.

Z	A	E_B^{exp} (MeV)	E_B^{calc} (MeV)	$E_B^{exp} - E_B^{calc}$ (MeV)	Z	A	E_B^{exp} (MeV)	E_B^{calc} (MeV)	$E_B^{exp} - E_B^{calc}$ (MeV)
34	70	39.4000	38.4792	0.9208	92	238	5.5000	5.6895	-0.1895
34	76	44.5000	44.7815	-0.2815	92	240	5.5000	6.4866	-0.9866
42	90	40.9200	41.7603	-0.8403	94	236	4.5000	4.5137	-0.0137
42	94	44.6800	45.1974	-0.5174	94	238	5.0000	4.5383	0.4617
42	98	45.8400	47.8580	-2.0180	94	240	5.1500	5.0469	0.1031
80	198	20.4000	22.1022	-1.7022	94	242	5.0500	5.7499	-0.6999
84	210	21.4000	22.2199	-0.8199	94	244	5.0000	6.4935	-1.4935
84	212	19.5000	20.4383	-0.9383	94	246	5.3000	7.1958	-1.8958
88	228	8.1000	7.8328	0.2672	96	242	5.0000	4.4339	0.5661
90	228	6.5000	6.9476	-0.4476	96	244	5.1000	5.1740	-0.0740
90	230	7.0000	6.0608	0.9392	96	246	4.8000	6.0138	-1.2138
90	232	6.2000	5.8163	0.3837	96	248	4.8000	6.6025	-1.8025
90	234	6.5000	5.5551	0.9449	96	250	4.4000	6.1782	-1.7782
92	232	5.4000	4.8495	0.5505	98	250	3.6000	6.0674	-2.4674
92	234	5.5000	5.0518	0.4482	98	252	4.8000	5.8170	-1.0170
92	236	5.6700	5.1745	0.4955					

3. The difference in energy between the symmetric and asymmetric saddle points in our calculated potential-energy surfaces is one to two MeV, which is consistent with the experimentally deduced differences.

4. The shapes we calculate for nuclei evolving in the mass-asymmetric and mass-symmetric valleys are consistent with the total fragment kinetic energies observed for these modes.

5. The long observed mass split in mass-asymmetric fission with an approximately constant heavy fragment mass near $A = 140$ is reproduced in our calculations.

6. Calculated fission-barrier heights agree very well with experimentally extracted barriers for nuclei from ^{70}Se to ^{252}Cf.

Except for Table 1 and the attendant discussion, these results have been obtained in our standard finite-range liquid-drop potential-energy model used for the calculation of nuclear masses. No change in the model or its parameters have been made in the current calculation, relative to its 1992 specification in Ref. [16]).

The calculations on which the results in this paper are based were carried out on the cluster of 4 CPUs at the TANDEM accelerator in JAERI in the winter of 1998–1999 and subsequently on the 140 processor AVALON cluster at Los Alamos. Results of the investigations at JAERI are discussed in Ref. [5]). This research is supported by the US DOE under contract W-7405-ENG-36.

References

1) E. Konecny, H. J. Specht, and J. Weber, Proc. Third IAEA Symp. on the Physics and Chemistry of Fission, Rochester, 1973, vol. II (IAEA, Vienna, 1974) p. 3.

2) Y. Nagame, I. Nishinaka, K. Tsukada, S. Ichikawa, H. Ikezoe, Y. L. Zhao, Y Oura, K. Sueki, H. Nakahara, M. Tanikawa, T. Ohtsuki, K. Takamiya, K. Nakanishi, H. Kudo, Y. Hamajima, and Y. H. Chung, Radiochimica Acta, **78** (1997) 3.

3) Y. L. Zhao, I. Nishinaka, Y. Nagame, M. Tanikawa, K. Tsukada, S. Ichikawa, K. Sueki, Y. Oura, H. Ikezoe, S. Mitsuoka, H. Kudo, T. Ohtsuki, and H. Nakahara, Phys. Rev. Lett. **82** (1999) 3408.

4) E. K. Hulet, J. F. Wild, R. J. Dougan, R. W. Lougheed, J. H. Landrum, A. D. Dougan, M. Schädel, R. L. Hahn, P. A. Baisden, C. M. Henderson, R. J. Dupzyk, K. Sümmerer, and G. R. Bethune, Phys. Rev. Lett. **56** (1986) 313.

5) P. Möller and A. Iwamoto, Phys. Rev. **C 61** (2000) 47602.

6) J. R. Nix, Nucl. Phys. **A130** (1969) 241.

7) S. Åberg, H. Flocard, and W. Nazarewicz, Ann. Rev. Nucl. Sci. **40**, 439 (1990).

8) J. L. Egido, L. M. Robledo, and R. R. Chasman, Phys. Lett. **B393**, 13 (1997).

9) J. F. Berger, M. Girod, and D. Gogny, Nucl. Phys. **A502**, c85 (1989).

10) A. Mamdouh, J. M. Pearson, M. Rayet, and F. Tondeur, Nucl. Phys. **A644** (1998) 389.

11) P. Möller, J. R. Nix, and W. J. Swiatecki, Nucl. Phys. **A469** (1987) 1.

12) P. Möller, J. R. Nix, and W. J. Swiatecki, Nucl. Phys. **A492** (1989) 349.

13) D. C. Hoffman and M. M. Hoffman, Ann. Rev. Nucl. Sci. **24** (1974) 151.

14) L. Dematte, C. Wagemans, R. Barthelemy, P. Dhondt, and A. Deruytter, Nucl. Phys. **A617** (1997) 331.

15) K.-H. Schmidt, S. Steinhäuser, C. Böckstiegel, A. Grewe, A. Heinz, A. R. Junghans, J. Benlliure, H.-G. Clerc, M. de Jong, J. Müller, M. Pfüntzer, and B. Voss, Nucl. Phys. **A665** (2000) 221.

16) P. Möller, J. R. Nix, W. D. Myers, and W. J. Swiatecki, Atomic Data Nucl. Data Tables **59** (1995) 185.